

Progress of Full- f Gyrokinetic Simulation Toward Reactor Relevant Numerical Experiments^{*)}

Yasuhiro IDOMURA, Motoki NAKATA¹⁾ and Sébastien JOLLIET²⁾

Japan Atomic Energy Agency, Kashiwanoha, 5-1-5 Kashiwa, Chiba 277-8587, Japan

¹⁾*Japan Atomic Energy Agency, Obuchi-Omotodate, 2-166 Rokkasho, Kamikita, Aomori 039-3212, Japan*

²⁾*Ecole Polytechnique Fédérale de Lausanne, Association Euratom-Switzerland, 1015 Lausanne, Switzerland*

(Received 21 November 2013 / Accepted 19 February 2014)

Full- f gyrokinetic simulations compute both turbulent transport and profile formations under fixed power, momentum, and particle input as in experiments. This approach has the capability of dictating plasma profiles, provided that time scale of the simulation is long enough to establish power, momentum, and particle balance conditions. Recent Peta-scale supercomputers made such long time scale simulations feasible, and full- f gyrokinetic simulations are applied to reactor relevant numerical experiments. In this paper, physical models, numerical approaches, and accuracy issues of the gyrokinetic full- f Eulerian code GT5D are summarized, and then, its recent applications to the scaling studies of turbulent transport with respect to plasma size and heating power are reviewed.

© 2014 The Japan Society of Plasma Science and Nuclear Fusion Research

Keywords: gyrokinetic theory, full- f Eulerian code, ion temperature gradient driven turbulence, plasma size scaling, power degradation of confinement

DOI: 10.1585/pfr.9.3503028

1. Introduction

In recent years, new generation of gyrokinetic simulations based on the so-called full- f approaches are emerging [1]. In full- f gyrokinetic simulations, both turbulent transport and profile formations are computed under fixed power, momentum, and particle inputs as in experiments. This approach, in principle, has the capability of dictating plasma profiles, provided that the simulation is performed over a confinement time, which is extremely longer than turbulent time scales, and that both the macroscopic plasma distribution f_0 and the microscopic turbulent fluctuation $\delta f \ll f_0$ are accurately computed by taking account of fast turbulent dynamics and slow collisional processes. However, such a multi-scale simulation requires wide ranging efforts from the development of numerical schemes and supercomputing techniques to various levels of verification studies on physical and numerical models. In this review, we summarize such efforts in the development of the gyrokinetic full- f Eulerian code GT5D [2].

In Ref. [3], GT5D was first applied to fixed flux ion temperature gradient driven (ITG) turbulence simulations, and various new phenomena such as self-organized critical phenomena in the ITG turbulence, avalanche like heat fluxes regulated by mean radial electric fields E_r , and the formation of intrinsic rotation were first disclosed based on first principles calculations. However, because of its large computational cost, the application of GT5D has been

mostly limited to small devices and/or short time scales, and the advantages of full- f approaches have not been fully utilized. In order to overcome this limitation, we have promoted the development of GT5D in two directions. One is to develop novel supercomputing techniques, which enables Peta-scale full- f gyrokinetic simulations. The other is to verify (and improve) physical models so that they have enough accuracy in confinement time scale numerical experiments. Through these efforts, the capability of GT5D has been significantly expanded with respect to problem sizes and time scales. In fact, recent Peta-scale supercomputers enable extreme scale full- f gyrokinetic simulations.

Compared with fixed gradient δf gyrokinetic simulations, fixed flux full- f gyrokinetic simulations have new physical effects such as turbulence suppression by mean E_r , neoclassical transport phenomena, interaction between turbulence and fluctuating temperature leading to self-organized critical phenomena, and so on. Among various physical effects, the most important difference may be a power balance condition [4]. In fixed gradient δf models, adaptive heat sources (and sinks) are imposed everywhere to fix temperature profiles on average, and the power balance is significantly affected by dynamic deposition profiles of adaptive sources. On the other hand, in fixed flux full- f models, the power balance is automatically established in source free regions, and turbulent heat transport and temperature profiles are evolved in a self-consistent manner. This feature is essential for computing stiff temperature profiles leading to the power degradation of confinement. By taking this advantage, we have stud-

author's e-mail: idomura.yasuhiro@jaea.go.jp

^{*)} This article is based on the invited presentation at the 23rd International Toki Conference (ITC23).

ied transport scalings with respect to plasma size and heating power, which are the most fundamental confinement scalings in the experiment [5], and critical for the ITER and future DEMO reactors, which are several times larger than the existing devices and have significantly larger self-heating than the present auxiliary heating.

The reminder of the paper is organized as follows. In Sec.2, calculation models and computational methods of GT5D are presented. In Sec.3, verification studies concerning to the accuracy of gyrokinetic models and the convergence of quasi-steady plasma profiles are explained. In Sec.4, recent works on the plasma size and power scaling of ITG turbulence are reviewed. Finally, a summary is given in Sec.5.

2. Calculation Model

We consider the electrostatic ITG turbulence described by gyrokinetic ions and adiabatic electrons in an axisymmetric toroidal configuration. GT5D is based on the modern gyrokinetic theory [6], in which the gyrokinetic equation is simply given as the Liouville equation,

$$\begin{aligned} \frac{Df}{Dt} &\equiv \frac{\partial f}{\partial t} + \{f, H\} \\ &= \frac{\partial f}{\partial t} + \dot{\mathbf{R}} \cdot \frac{\partial f}{\partial \mathbf{R}} + v_{\parallel} \frac{\partial f}{\partial v_{\parallel}} = 0, \end{aligned} \quad (1)$$

using the gyro-centre Hamiltonian,

$$H = \frac{1}{2} m_i v_{\parallel}^2 + \mu B + e \langle \phi \rangle_{\alpha}, \quad (2)$$

and the gyrokinetic Poisson bracket operator,

$$\begin{aligned} \{F, G\} &\equiv \frac{\Omega_i}{B} \left(\frac{\partial F}{\partial \alpha} \frac{\partial G}{\partial \mu} - \frac{\partial F}{\partial \mu} \frac{\partial G}{\partial \alpha} \right) \\ &+ \frac{\mathbf{B}^*}{m_i B_{\parallel}^*} \cdot \left(\nabla F \frac{\partial G}{\partial v_{\parallel}} - \frac{\partial F}{\partial v_{\parallel}} \nabla G \right) \\ &- \frac{c}{e B_{\parallel}^*} \mathbf{b} \cdot \nabla F \times \nabla G, \end{aligned} \quad (3)$$

in the gyro-centre coordinates $\mathbf{Z} = (t; \mathbf{R}, v_{\parallel}, \mu, \alpha)$. Here, \mathbf{R} is a position of the guiding centre, v_{\parallel} is the parallel velocity, μ is the magnetic moment, α is the gyro-phase angle, $\mathbf{B} = B\mathbf{b}$ is the magnetic field, \mathbf{b} is the unit vector in the parallel direction, m_i and e are the mass and charge of ions, respectively, c is the velocity of light, $\Omega_i = (eB)/(m_i c)$ is the cyclotron frequency, $B_{\parallel}^* = \mathbf{b} \cdot \mathbf{B}^*$ is a parallel component of $\mathbf{B}^* = \mathbf{B} + (Bv_{\parallel}/\Omega_i)\nabla \times \mathbf{b}$, ϕ is the electrostatic potential, and the gyro-averaging operator is defined as $\langle \cdot \rangle_{\alpha} \equiv \oint \cdot d\alpha/2\pi$. The nonlinear characteristics $\dot{\mathbf{Z}} = \{\mathbf{Z}, H\}$ are given as

$$\begin{aligned} \dot{\mathbf{R}} &= v_{\parallel} \mathbf{b} \\ &+ \frac{c}{e B_{\parallel}^*} \mathbf{b} \times \left(e \nabla \langle \phi \rangle_{\alpha} + m_i v_{\parallel}^2 \mathbf{b} \cdot \nabla \mathbf{b} + \mu \nabla B \right), \end{aligned} \quad (4)$$

$$\dot{v}_{\parallel} = - \frac{\mathbf{B}^*}{m_i B_{\parallel}^*} \cdot \left(e \nabla \langle \phi \rangle_{\alpha} + \mu \nabla B \right). \quad (5)$$

By using the phase space volume conservation $\nabla \cdot (\mathcal{J}\dot{\mathbf{R}}) + \partial_{v_{\parallel}} (\mathcal{J}\dot{v}_{\parallel}) = 0$, the gyrokinetic equation (1) yields its con-

servative form,

$$\frac{\partial \mathcal{J}f}{\partial t} + \nabla \cdot (\mathcal{J}\dot{\mathbf{R}}f) + \frac{\partial}{\partial v_{\parallel}} (\mathcal{J}\dot{v}_{\parallel}f) = 0, \quad (6)$$

where $\mathcal{J} = m_i^2 B_{\parallel}^*$ is the Jacobian of the gyro-centre coordinates. By adding a collision term $C(f)$, a source term S_{src} , and a sink term S_{snk} , a conservative gyrokinetic equation used in GT5D is written as,

$$\begin{aligned} \frac{\partial \mathcal{J}f}{\partial t} + \nabla \cdot (\mathcal{J}\dot{\mathbf{R}}f) + \frac{\partial}{\partial v_{\parallel}} (\mathcal{J}\dot{v}_{\parallel}f) \\ = \mathcal{J}C(f) + \mathcal{J}S_{\text{src}} + \mathcal{J}S_{\text{snk}}. \end{aligned} \quad (7)$$

Ion-ion collisions are computed using a linear Fokker-Planck collision operator [7]. The source term can be flexibly changed from a δf like fixed gradient model to a full- f fixed flux model, where heat and momentum sources are independently controlled [4, 8]. In a standard on-axis heating condition, auxiliary heating is given by $S_{\text{src}} = \nu_h A_{\text{src}}(r)(f_{M1} - f_{M2})$, where a deposition profile $A_{\text{src}}(r)$ is distributed in the plasma core. Here, r is the radial coordinate. The heating rate ν_h and two Maxwellian distribution functions with different temperatures, f_{M1}, f_{M2} , are chosen to impose fixed power input P_{in} with no particle and momentum input. On the other hand, an L-mode like boundary condition with a fixed edge temperature and no slip boundary is imposed by a Krook type sink operator $S_{\text{snk}} = \nu_s A_{\text{snk}}(r)(f - f_0)$, where f_0 is the initial distribution function, $A_{\text{snk}}(r)$ is localized near the plasma surface, and a typical sink parameter $\nu_s \sim 0.1v_{ti}/a$ is chosen to fix the edge temperature and rotation.

The self-consistency is imposed by the gyrokinetic Poisson equation,

$$\begin{aligned} -\nabla_{\perp} \cdot \frac{\rho_{ti}^2}{\lambda_{Di}^2} \nabla_{\perp} \phi + \frac{1}{\lambda_{De}^2} (\phi - \langle \phi \rangle_f) \\ = 4\pi e \left[\int f \delta([\mathbf{R} + \boldsymbol{\rho}] - \mathbf{x}) d^6 Z - n_{0e} \right], \end{aligned} \quad (8)$$

where $\mathbf{R} + \boldsymbol{\rho}$ is a particle position, $d^6 Z = m_i^2 B_{\parallel}^* d\mathbf{R} dv_{\parallel} d\mu d\alpha$ is the phase space volume of the gyro-centre coordinates, ρ_{ti} is the Larmor radius evaluated with the thermal velocity v_{ti} , λ_{Di} and λ_{De} are the ion and electron Debye lengths, and $\langle \cdot \rangle_f$ is a flux surface average operator. In Eq. (8), we use a linearised ion polarisation term with a long wavelength approximation, which is valid for the core ITG turbulence characterised by $k_{\perp}^2 \rho_{ti}^2 \ll 1$ and $\delta n/n_0 \ll 1$. The gyrokinetic equations (2) and (8) are derived from the standard first order gyrokinetics, and keep the so-called energetic consistency, which guarantees the energy and toroidal angular momentum conservation laws [9].

In GT5D, the gyrokinetic Poisson bracket operator in Eq. (1) is discretized using a fourth order non-dissipative conservative finite difference scheme [2, 10], which enables robust and accurate computation of nonlinear turbulent dynamics based on a full- f approach. The gyrokinetic Poisson equation (8) is computed using toroidal mode expansion and a 2D finite element approximation on the poloidal

plane. The resulting finite element equation is treated by a field-aligned gyrokinetic Poisson solver, which dramatically reduces scaling of the memory usage from $\sim \rho^{*-3}$ to $\sim \rho^{*-1}$ [11], where $\rho^* = \rho_{ti}/a$ and a is the minor radius. The linear Fokker-Planck collision operator is discretized using a sixth order centred finite difference scheme, and a conservative field particle operator [12] is implemented to keep an exact conservation of the particle, momentum, and energy moments. The time integration is performed using the second order additive semi-implicit Runge-Kutta method [13] and a stiff linear term involving the parallel streaming is treated implicitly using a generalized conjugate residual method [14].

The accuracy of collisionless turbulent dynamics of GT5D was verified through linear and nonlinear ITG benchmark tests against a gyrokinetic δf particle code GT3D [2]. While the latter benchmark was comparisons of decaying ITG turbulence simulations, in Ref. [4], it was confirmed that in a local limit regime ($\rho^{*-1} = 450$), GT5D with the δf like fixed gradient model recovers transport levels of local flux-tube gyrokinetic simulations with a gyrokinetic flux-tube Eulerian code GKV [15]. On the other hand, the neoclassical physics was tested in benchmark calculations against a neoclassical δf particle code FORTEC-3D [12]. Recently, a hybrid kinetic electron model [16] was added to GT5D and linear ITG and trapped electron mode (TEM) calculations were compared against a gyrokinetic flux-tube Eulerian code GKW [17]. This comparison clarified the so-called profile shear residual stress and its transition between ITG and TEM turbulence [18].

The code is highly parallelized using a multi-

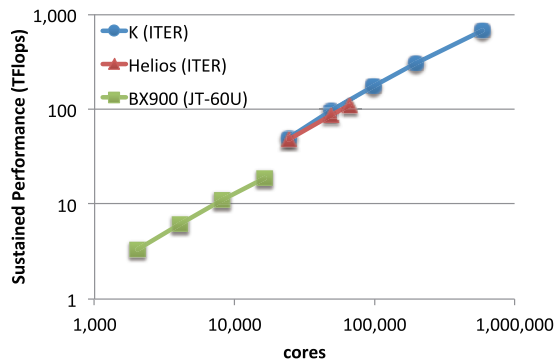


Fig. 1 Strong scaling of GT5D on the BX900 at the JAEA (Nehalem-EP and InfinibandQDR), the Helios at the IFERC (SandyBridge-EP and InfinibandQDR), and the K-computer at the Riken (Sparc64VIIIfx and Tofu interconnect). Problem sizes for JT-60U ($N_R \times N_\zeta \times N_Z \times N_{v\parallel} \times N_{v\perp} = 240 \times 64 \times 240 \times 128 \times 32 \sim 1.5 \times 10^{10}$) and ITER ($768 \times 64 \times 768 \times 128 \times 32 \sim 1.5 \times 10^{11}$) are used. Compared with the maximum performance of the BX900 with 16,384 cores, $\times 35$ ($\times 5.8$) speed up is achieved using 589,824 cores on the K-computer (65,536 cores on the Helios). Parallel efficiency of $\sim 99.99989\%$ is achieved on the K-computer.

dimensional domain decomposition, which is designed based on physical symmetry properties of the gyrokinetic operator (μ symmetry), the collision operator (\mathbf{R} symmetry), and the Poisson operator (toroidal symmetry) [19]. The domain decomposition model is implemented using a hybrid parallelization model consisting of multi-layer MPI communicators and multi-core OpenMP parallelization. In addition, a novel computation and communication overlap technique [20] is developed using communication threads, which are implemented with a heterogeneous OpenMP programming model. The strong scaling of GT5D is dramatically improved by this latency hiding technique, and on the K-computer, an excellent strong scaling is achieved up to ~ 0.6 million cores (see Fig. 1). Thanks to the Peta-scale computing capability, space and time scales accessible via GT5D are significantly expanded, and extreme scale simulations such as ITER size simulations and confinement time scale simulations are enabled.

3. Verification of GT5D

In this section, we review recent verification studies with respect to the accuracy of gyrokinetic models, and the convergence of steady state profiles. In Ref. [21], a serious concern was raised concerning the accuracy of momentum transport calculations using the first order gyrokinetics, in particular, with full- f approaches. This argument was based on the so-called recursive approach [22], and by assuming gyro-Bohm diffusion for small toroidal rotation following a low flow ordering $U_\varphi/v_{ti} \sim \rho^*$, it was shown that in order to satisfy the toroidal angular momentum conservation, one needs to determine the quasi-neutrality condition up to third-order accuracy with respect to ρ^* . Here, U_φ is the toroidal rotation velocity. However, most of the existing gyrokinetic simulations are based on the first order gyrokinetics, and the above requirement is not satisfied.

On the other hand, apart from the above classical ordering arguments, Ref. [9] clearly demonstrated that the toroidal angular momentum conservation is guaranteed at any order, provided that the equation system is derived based on modern gyrokinetic theory [6] with an energetic consistency. In contrast to the recursive approach, in which f is expanded using the gyrokinetic ordering, in modern gyrokinetic theory, a perturbation theory is applied to the Hamiltonian or the field Lagrangian, and after truncating it, the equation system is derived while keeping relevant symmetry and conservation properties. Therefore, gyrokinetic simulations based on modern gyrokinetic theory may not be subject to the above critique. However, the remaining concern was whether there exists erroneous momentum transport satisfying the toroidal angular momentum conservation. In order to resolve this critical issue, third order gyrokinetics [23] was implemented on GT5D, and the quantitative convergence of turbulent momentum transport with respect to the gyrokinetic ordering is examined in the ITG turbulence [24]. Here, the third order gyrokinetics is

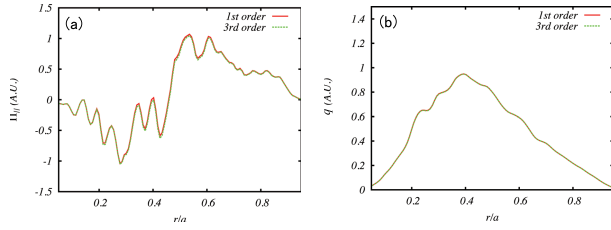


Fig. 2 Comparisons of (a) the parallel momentum flux Π_{\parallel} and (b) the heat flux q computed using first and third order gyrokinetic models [24]. The data is observed in ITG turbulence simulations (Cyclone parameter, $P_{\text{in}} = 2 \text{ MW}$, $\rho^{*-1} = 150$).

derived using a long wavelength approximation, and the gyro-center Hamiltonian is given as

$$H = \frac{1}{2} m_i v_{\parallel}^2 + \mu B + e \langle \phi \rangle_{\alpha} - \frac{m_i c^2}{2B^2} (\nabla_{\perp} \phi)^2 + \frac{e}{2} (\nabla_{\perp} \phi \cdot \nabla_{\perp}) \left(\frac{P_E^2}{2} \right), \quad (9)$$

where $P_E = -m_i c^2 / e B^2 \nabla_{\perp} \phi$ is the polarization vector.

Figure 2 shows comparisons of turbulent transport in the ITG turbulence simulations (Cyclone parameter [25], $P_{\text{in}} = 2 \text{ MW}$, $\rho^{*-1} = 150$) computed using first and third order gyrokinetic models. Here, the third order fluxes are computed as test particle transport. The results show negligible differences both for turbulent heat and momentum fluxes (relative errors of $\sim 0.2\%$ and $\sim 4\%$, respectively). This is explained by the following ordering argument. In the ITG turbulence, where long wavelength spectra with $k_{\perp}^2 \rho_{\text{ti}}^2 \ll 1$ are dominant, the second and third order correction terms (the fourth and fifth terms in Eq. (9)) become two and four orders of magnitudes smaller than those for arbitrary wavelength perturbations. In addition, in a global gyrokinetic model, profile shearing due to density and temperature profiles induces the profile shear residual stress, which scales as $\propto \rho^{*1/3}$ [18]. Because of such symmetry breaking effects, non-diffusive momentum transport and the resulting intrinsic rotation velocity often greatly exceeds the low flow ordering. These corrections lead to converged momentum transport calculations even with the standard first order gyrokinetics.

Another important concern is the convergence of full- f gyrokinetic simulations with respect to time. Although confinement time scale simulations can determine steady plasma profiles based on first principles, such long time simulations are extremely costly for experimentally relevant machine sizes, and most of full- f gyrokinetic simulations were operated for a few collision times. One may observe *quasi-steady* turbulent fluctuations even in such short time simulations. However, plasma profiles, which drive and suppress turbulence, may not be in *steady* states, and transport levels may not be converged yet. To answer this question, confinement time scale full- f simulations are performed using GT5D, and the convergence of steady

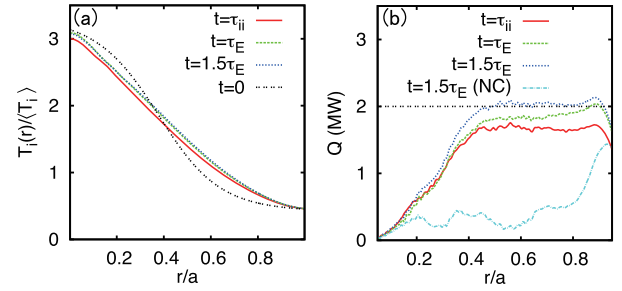


Fig. 3 Time evolutions of (a) the normalized ion temperature $T_i / \langle T_i \rangle$ ($\langle T_i \rangle$ is a volume averaged temperature at $t = 0$) and (b) the total (neoclassical and turbulent) heat flux integrated over the magnetic surface Q in a long time ITG turbulence simulation (Cyclone parameter, $P_{\text{in}} = 2 \text{ MW}$, $\rho^{*-1} = 100$) [26]. In (b), the neoclassical (NC) fraction of Q in the steady state is also plotted.

state plasma profiles is examined [26].

Figure 3 shows the time evolutions of the ion temperature and the total (neoclassical and turbulent) heat flux integrated over the magnetic surface Q in the long time ITG turbulence simulation (Cyclone parameter, $P_{\text{in}} = 2 \text{ MW}$, $\rho^{*-1} = 100$). In the simulation, the ion-ion collision time is $\tau_{\text{ii}} \sim 3 \text{ ms}$ and the core energy confinement time $\tau_E = W_{\text{core}} / P_{\text{in}}$ is estimated as $\tau_E \sim 12 \text{ ms}$. In computing the core ion stored energy W_{core} , a part of the ion stored energy sustained by the boundary temperature is subtracted from the total stored energy. The initial temperature profile is set as $R/L_{\text{ti}} = 10$, which is far above linear and non-linear thresholds at $R/L_{\text{ti}} \sim 4.5$ and at $R/L_{\text{ti}} \sim 6$, respectively [2]. Here, R is the major radius and L_{ti} is the ion temperature gradient scale length. Such a linearly unstable initial condition leads to strong excitation of linear ITG modes followed by initial transient bursts, which accelerate temperature relaxation processes towards steady states. As a result, the power balance condition is established in much shorter time scale than τ_E , and the total heat flux quantitatively matches the input power ($Q \sim P_{\text{in}}$) in the source free region. In Fig. 3 (b), the increase and decrease of Q for $r/a < 0.5$ and $r/a > 0.9$ correspond to the deposition profiles of the on-axis heating and the sink term in the edge. The neoclassical fraction of Q is an order of magnitude smaller than the turbulent fraction, while it increases in the edge, where collisional effects due to the Krook type sink operator enhances the neoclassical transport. The core stored energy is saturated after $t \sim \tau_E \sim 10 \text{ ms}$, and the quantitative convergence of temperature profiles is observed in the steady state. However, even after τ_{ii} , the temperature profile is qualitatively similar to converged one, and the power balance is approximately satisfied within 10 \sim 20% differences from P_{in} (see Fig. 3 (b)). It was also confirmed that after a few collision times, the variance of transport levels and temperature gradients drops to a few per cent [8]. These observations support the relevance of earlier shorter time scale simulations.

4. Plasma Size and Power Scaling

The plasma size scaling of turbulent heat transport is of critical importance in predicting performances of future fusion devices. Although this issue was addressed experimentally [27], plasma size parameters of existing devices are far below reactor relevant regimes, and extrapolations of transport properties play critical roles in the reactor design studies [5]. On the other hand, with rapidly increasing computing power, the credibility of gyrokinetic simulations has dramatically improved, and the plasma size scaling of turbulent transport has also been theoretically investigated based on numerical experiments with global gyrokinetic simulations.

In Ref. [28], the plasma size scaling of the ion temperature gradient driven (ITG) turbulence was first addressed using a δf gyrokinetic particle code, and the transition of transport scaling from a Bohm like scaling to a gyro-Bohm like scaling was found for large devices. In Ref. [29], a key mechanism was proposed as spreading of turbulent fluctuations into linearly stable core and edge regions, which were prescribed in the simulation. In Ref. [30], the transition feature and saturation levels of the above transport scaling were quantitatively verified from comparisons of δf gyrokinetic particle and Eulerian codes and of different MHD equilibrium models, and the transport scaling was explained by profile shearing, which is characterized by the effective plasma size or the size of high temperature gradient region.

Although several δf gyrokinetic simulations give the converged transport scaling, it may not be experimentally relevant from the viewpoint of heating power. In plasma size scans with fixed gradient δf gyrokinetic simulations, the plasma size ρ^{*-1} is varied with the fixed normalized temperature gradient R/L_{Ti} . If one computes heat sources based on a power balance in such a situation, a Bohm like scaling means increasing power input with the plasma size, while a gyro-Bohm like scaling corresponds to constant power input regardless of the plasma size. Therefore, the size scaling studies based on δf gyrokinetic simulations implicitly involve influences of heating power on turbulent transport or the power scaling, which significantly affects global confinement scalings [5]. In addition, the gyro-Bohm like scaling may not be relevant for future large devices, in which total heating power including self-heating by the fusion-generated alpha particles will be significantly larger than auxiliary heating in the present experiments.

To address the above fundamental question, we have revisited the plasma size scaling of ITG turbulence using fixed-flux full- f gyrokinetic simulations, where both plasma size and heating power are scaled. In Ref. [8], the plasma size and power scaling of ITG turbulence was first investigated for small devices, where the heating power was chosen to be proportional to ρ^{*-1} based on the former size scaling experiments [27]. The plasma size scan is performed for Cyclone parameters with $(\rho^{*-1}, P_{in}) = (100, 1.33 \text{ MW}), (150, 2 \text{ MW}), \text{ and } (225, 3 \text{ MW})$. The initial

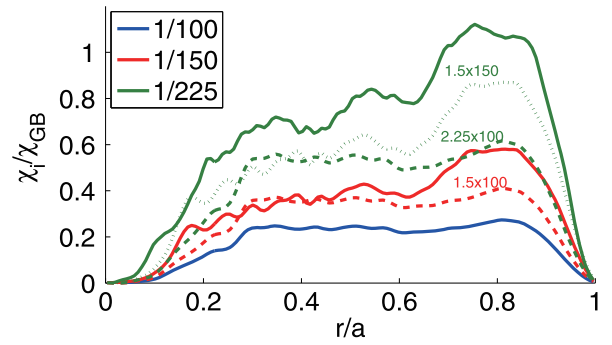


Fig. 4 Radial profiles of the normalized ion heat diffusivity χ_i/χ_{GB} ($\chi_{GB} = \rho_{ii}^2 \nu_{ii}/L_n$ is defined by $\langle T_i \rangle(t=0)$) observed in the plasma size scaling numerical experiments with $(\rho^{*-1}, P_{in}) = (100, 1.33 \text{ MW}), (150, 2 \text{ MW}), \text{ and } (225, 3 \text{ MW})$ (Cyclone parameter) [8]. Green and red dashed curves show Bohm like extrapolations (proportional to $1/\rho^*$) from $1/\rho^* = 100$ to $1/\rho^* = 150$ and $1/\rho^* = 150$ to $1/\rho^* = 225$, respectively. A green dotted curve is a Bohm like extrapolation from $1/\rho^* = 150$ to $1/\rho^* = 225$. The ion heat diffusivity observed in the numerical experiment (solid curves) exceeds these estimations, and the so-called worse-than-Bohm scaling is observed.

condition is given by the aforementioned linearly unstable condition, and a typical simulation period is $\sim 2000R/\nu_{ii}$ ($\sim 4\tau_{ii}$). Figure 4 shows the normalized ion heat diffusivity χ_i/χ_{GB} observed in the quasi-steady states. It is noted that in Ref. [31], the so-called short fall problem was reported, and in the outer region of L-mode plasma, heat fluxes predicted from δf flux-tube gyrokinetic simulations were significantly lower than the experiment. However, in the present full- f simulation, the power balance condition is automatically satisfied as shown in Fig. 3 (b), and the ion heat diffusivity tends to increase toward the edge as in the experiment. Therefore, such a short fall problem is not likely to occur, provided that the deposition profile of heat source is chosen based on the experiment.

The numerical experiments indicate the so-called worse-than-Bohm scaling with $\chi_i/\chi_{GB} \propto \rho^{*-1.66}$, which is rather close to the observation in the size scaling L-mode experiments on DIII-D, $\chi_i/\chi_{GB} \propto \rho^{*-1.5 \pm 0.3}$ [27]. In the numerical experiments, a gyro-Bohm like scaling of turbulent fluctuations is simultaneously recovered with the correlation length of $\Delta r \sim 5\rho_{ii}$ and the correlation time of $\Delta t \sim 2a/c_s$, which also agree with the size scaling experiments [32]. Here, c_s is the ion sound velocity. To understand transport mechanisms leading to the worse-than-Bohm scaling, the numerical experiments are analyzed from the various viewpoints such as characteristics of avalanche like non-local transport and turbulence suppression due to mean E_r shear, which is determined by a radial force balance. Although these transport mechanisms vary depending on ρ^* , their scalings are not enough for explaining the worse-than-Bohm scaling of turbulent transport.

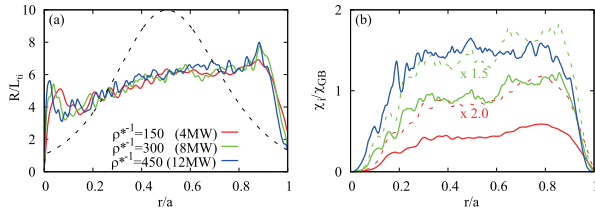


Fig. 5 Radial profiles of (a) R/L_{ti} and (b) the normalized ion heat diffusivity χ_i/χ_{GB} ($\chi_{GB} = \rho_{ti}^2 \nu_{ti}/L_n$ is defined by $T_i(t) \sim 1.34\langle T_i \rangle(t=0)$) observed in the extended plasma size scan with $(\rho^{*-1}, P_{in}) = (150, 4 \text{ MW})$, $(300, 8 \text{ MW})$, and $(450, 12 \text{ MW})$ (Cyclone parameter) [4]. In (a), the initial temperature gradient with $R/L_{ti} = 10$ at midradius is plotted with dashed lines. In (b), red and green dashed curves show Bohm like extrapolations (proportional to $1/\rho^*$) from $1/\rho^* = 150$ to $1/\rho^* = 300$ and from $1/\rho^* = 300$ to $1/\rho^* = 450$, respectively.

In order to understand this open question, in Refs. [4], we have extended the plasma size up to the local limit regime or $\rho^{*-1} > 300$, where δf gyrokinetic simulations predict a gyro-Bohm like scaling and finite ρ^* effects such as profile shearing are expected to be small enough. In the extended plasma size scan, plasma size and heating power are chosen as $(\rho^{*-1}, P_{in}) = (150, 4 \text{ MW})$, $(300, 8 \text{ MW})$, and $(450, 12 \text{ MW})$. These parameters give a Bohm like scaling or χ_i/χ_{GB} proportional to the plasma size, provided that R/L_{ti} is unchanged. By using the above parameters, one can clearly test two extreme situations, increasing (Bohm like) χ_i/χ_{GB} with constant R/L_{ti} and constant (gyro-Bohm like) χ_i/χ_{GB} with increasing R/L_{ti} , which are different from the situation of δf simulations: constant χ_i/χ_{GB} with constant R/L_{ti} for $\rho^{*-1} > 300$.

Figure 5 shows χ_i/χ_{GB} and R/L_{ti} observed in a series of numerical experiments. The ion temperature gradient falls down from the initial condition $R/L_{ti} = 10$ to the quasi-steady state $R/L_{ti} \sim 6$, which is limited by the nonlinear critical gradient. Because of the stiff ion temperature profiles, χ_i/χ_{GB} increases with the plasma size following the power balance. Unlike former δf simulations, the present numerical experiments show increasing χ_i/χ_{GB} with the similar R/L_{ti} even in the local limit regime. It is noted that the local flux-tube gyrokinetic Eulerian code GKV [15] gives $\chi_i/\chi_{GB} \sim 2.5$ at $R/L_{ti} = 6$. Compared with this local limit value, present full- f simulations tend to give lower transport levels in the local limit regime. This tendency was found also in the former benchmark study [33], where full- f simulations used significantly higher temperature gradients $R/L_{ti} \sim 10$ to reach at transport levels of δf simulations with $R/L_{ti} \sim 7$.

For large devices with $\rho^{*-1} > 300$, profile shearing due to density, temperature, and mean E_r decreases with the plasma size, and a dominant shearing effect comes from turbulence driven zonal flows E_{ZF} , which has meso-scale structures with similar scale lengths $\sim 20\rho_{ti}$ regardless of the plasma size. Heat fluxes show non-local trans-

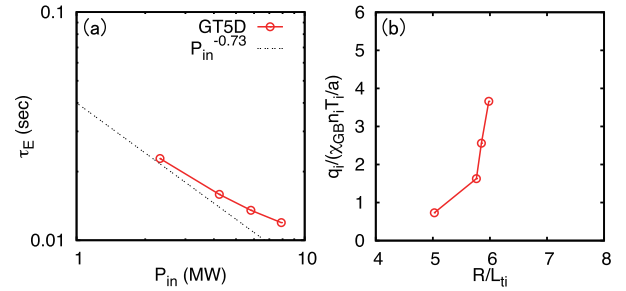


Fig. 6 (a) power scaling of the core energy confinement time τ_E and (b) R/L_{ti} dependence of the heat flux q ($r/a = 0.5$) observed in the power scan with $P_{in} = 2 \sim 8 \text{ MW}$ (Cyclone parameter, $\rho^{*-1} = 150$) [34]. In (a), the power scaling of L-mode experiments, $\tau_E \propto P_{in}^{-0.73}$ [5], is plotted with a dashed line.

port due to radial propagation of avalanches, and indicate self-organized critical phenomena such as $1/\omega$ frequency spectra. Low amplitude avalanches below the time-averaged transport level are typically trapped by a single zone of E_{ZF} , their propagation directions are determined by the sign of E_{ZF} shear, and the propagation widths show a gyro-Bohm like dependency. On the other hand, large amplitude bursts propagate over significant radii across multiple zones of E_{ZF} . Such large scale avalanches carry about $\sim 70\%$ of turbulent heat transport. Large scale avalanches are followed by quiescent phases, and transient drop and build-up of the temperature gradient are repeated following a local power balance. This process leads to higher super-critical states and larger amplitude bursts at smaller ρ^* (and higher P_{in}), and gives different transport levels with the similar time-averaged temperature gradients. This transport property in the local limit regime can not be explained by the conventional plasma size effects such as profile shearing and turbulence spreading.

To understand the transport property, which produces stiff temperature profiles and the Bohm like scaling of turbulent transport, in Ref [34], we have addressed influences of heating power on the transport scaling or the power degradation of confinement, and the relation between the above transport scaling and the power scaling is investigated through systematic power scans with fixed ρ^* . Figure 6 shows the power scaling of τ_E and the stiffness of ion temperature profiles observed in the power scan with $\rho^{*-1} = 150$. The degradation of confinement is observed with increasing heating power, and the power scaling with $\tau_E \propto P_{in}^{-0.55}$, which shows the similar tendency as the power scaling of L-mode experiments, $\tau_E \propto P_{in}^{-0.73}$ [5], is successfully recovered.

In the power scan, it is clearly seen that a nonlinear critical gradient exists at $R/L_{ti} \sim 6$ [2, 25], and the heat flux rapidly increases when the temperature gradient exceeds the nonlinear critical gradient. This feature provides stiff ion temperature profiles leading to the power degradation of confinement. It is noted that in the lowest power

case, neoclassical and turbulent heat fluxes are comparable, and such criticality does not appear. From detailed comparisons of the simulation data, it is shown that the extended plasma size scan and the power scan show the similar stiffness of ion temperature profiles or the similar dependency of q on R/L_{ti} . In addition, the probability distribution functions (PDFs) of q also show similar extensions of non-Gaussian tail components depending on P_{in} . From these observations, it is found that when heating power is scaled with plasma size, the transport scaling for large devices in the local limit regime is dominated by the power scaling or the power degradation of confinement.

5. Summary

In this review, recent progress of the full- f gyrokinetic Eulerian code GT5D toward reactor relevant numerical experiments is summarized. By developing novel supercomputing techniques, which enable us to fully utilize the latest Peta-scale resources, the capabilities of full- f gyrokinetic simulations are significantly expanded with respect to problem sizes and time scales. In addition to the computing power, careful verification studies support the physical soundness of such extreme scale numerical experiments. By taking advantage of fixed flux nature of full- f gyrokinetic simulations, the power degradation of confinement is first shown by first principles simulations, and it is clarified that the stiffness of temperature profiles dictates the power scaling of turbulent transport. Based on this knowledge, a puzzling issue on the relation between the plasma size scaling and the power scaling is addressed, and it is found that the transport scaling of large devices may strongly depend on heating power. Although former δf gyrokinetic simulations reported that the plasma size scaling of turbulent transport in large devices will be gyro-Bohm like, actual transport scaling may be significantly different if one takes account of heating power, which will be significantly larger in the ITER and DEMO reactors than the present devices. In the present ρ^* scan, the transport level is still lower than the flux-tube limit, but it may be further increased if the power degradation of global confinement occurs. In future works, the power scaling in reactor relevant plasma sizes will be addressed.

Acknowledgments

The computation in this work was performed on the BX900 at the JAEA, the Helios at the IFERC, and the K-computer at Riken. The authors would like to thank Dr. Y. Camenen for fruitful discussions on the profile shear residual stress. They are also grateful to Drs. H. Sugama, T.-H. Watanabe, and L. Villard for useful discussions on the plasma size scaling. This work is supported by the MEXT, Grant for HPCI Strategic Program Field No.4: Next-Generation Industrial Innovations, and Grant No. 22866086.

- [1] X. Garbet, Y. Idomura, L. Villard and T.H. Watanabe, Nucl. Fusion **50**, 043002 (2010).
- [2] Y. Idomura, M. Ida, T. Kano *et al.*, Comput. Phys. Commun. **179**, 391 (2008).
- [3] Y. Idomura, H. Urano, N. Aiba and S. Tokuda, Nucl. Fusion **49**, 065029 (2009).
- [4] M. Nakata and Y. Idomura, Nucl. Fusion **53**, 113039 (2013).
- [5] ITER Physics Expert Groups on Confinement and Transport and Confinement Modelling and Database, ITER Physics Basis Editors and ITER EDA, Nucl. Fusion **39**, 2175 (1999).
- [6] A.J. Brizard and T.S. Hahm, Rev. Mod. Phys. **79**, 421 (2007).
- [7] X.Q. Xu and M.N. Rosenbluth, Phys. Fluids B **3**, 627 (1991).
- [8] S. Jolliet and Y. Idomura, Nucl. Fusion **52**, 023026 (2012).
- [9] B. Scott and J. Smirnov, Phys. Plasmas **17**, 112302 (2010).
- [10] Y. Idomura, M. Ida, S. Tokuda and L. Villard, J. Comput. Phys. **226**, 244 (2007).
- [11] S. Jolliet, B.F. McMillan, L. Villard *et al.*, J. Comput. Phys. **231**, 745 (2012).
- [12] S. Satake, Y. Idomura, H. Sugama and T.-H. Watanabe, Comput. Phys. Commun. **181**, 1069 (2010).
- [13] X. Zhong, J. Comput. Phys. **128**, 19 (2007).
- [14] S.C. Eisenstat, H.C. Elman and M. Schultz, SIAM J. Num. Anal. **20**, 345 (1983).
- [15] T.-H. Watanabe and H. Sugama, Nucl. Fusion **46**, 24 (2006).
- [16] Y. Idomura, S. Tokuda and Y. Kishimoto, J. Plasma Fusion Res. SERIES **6**, 17 (2004).
- [17] A.G. Peeters, Y. Camenen, F.J. Casson *et al.*, Comput. Phys. Commun. **180**, 2650 (2009).
- [18] Y. Camenen, Y. Idomura, S. Jolliet and A.G. Peeters, Nucl. Fusion **51**, 073039 (2011).
- [19] Y. Idomura and S. Jolliet, In Proceedings of SC11, Seattle, USA (2011).
- [20] Y. Idomura, M. Nakata, S. Yamada *et al.*, Int. J. High Perform. Comput. Appl. **28**, 73 (2014).
- [21] F.I. Parra and P.J. Catto, Phys. Plasmas **17**, 056106 (2010).
- [22] E.A. Frieman and L. Chen, Phys. Fluids **25**, 502 (1982).
- [23] A. Mishchenko and A.J. Brizard, Phys. Plasmas **18**, 022305 (2011).
- [24] Y. Idomura, Comput. Sci. Disc. **5**, 014018 (2012).
- [25] A.M. Dimits, G. Beteman, M.A. Beer *et al.*, Phys. Plasmas **7**, 969 (2000).
- [26] Y. Idomura, Phys. Plasmas **21**, 022517 (2014).
- [27] C.C. Petty, T.C. Luce, R.I. Pinsky *et al.*, Phys. Rev. Lett. **74**, 1763 (1995).
- [28] Z. Lin, S. Ethier, T.S. Hahm and W.M. Tang, Phys. Rev. Lett. **88**, 195004 (2002).
- [29] T.S. Hahm, P.H. Diamond, Z. Lin *et al.*, Plasma Phys. Control. Fusion **46**, A323 (2004).
- [30] B.F. McMillan, X. Lapillonne, S. Brunner *et al.*, Phys. Rev. Lett. **105**, 155001 (2010).
- [31] T.L. Rhodes, C. Holland, S.P. Smith *et al.*, Nucl. Fusion **51**, 063022 (2011).
- [32] G.R. McKee, C.C. Petty, R.E. Waltz *et al.*, Nucl. Fusion **41**, 1235 (2001).
- [33] Y. Sarazin, V. Grandgirard, J. Abiteboul *et al.*, Nucl. Fusion **51**, 103023 (2011).
- [34] Y. Idomura and M. Nakata, Phys. Plasmas **21**, 020706 (2014).